

Inelastic electron-exciton scattering in bulk germaniumM. Stein,^{*} F. Schäfer, and L. Gomell*Department of Physics and Material Sciences Center, Philipps-Universität Marburg, Renthof 5, 35032 Marburg, Germany*

(Received 28 February 2019; revised manuscript received 9 April 2019; published 25 April 2019)

We investigate the destructive inelastic as well as the elastic scattering of a hot electron-hole plasma with an incoherent exciton population in bulk Ge by means of optical pump-terahertz probe spectroscopy. An incoherent exciton population evolves from a first optical pulse while a delayed second optical pulse creates the electron-hole plasma. The interaction of the plasma with the exciton population is monitored via the intraexcitonic transitions by a probing terahertz pulse. Analyzing the density-dependent decay of the intraexcitonic transitions after the arrival of the second optical pulse yields an inelastic scattering rate of $2.0 \times 10^{-4} \text{ cm}^3 \text{ s}^{-1}$. An analysis of the corresponding linewidth of the $1s - 2p$ transition yields a total scattering rate of $3.7 \times 10^{-4} \text{ cm}^3 \text{ s}^{-1}$. This allows us to experimentally distinguish between elastic and inelastic scattering and we obtain an elastic scattering rate of $1.7 \times 10^{-4} \text{ cm}^3 \text{ s}^{-1}$.

DOI: [10.1103/PhysRevB.99.144310](https://doi.org/10.1103/PhysRevB.99.144310)**I. INTRODUCTION**

Carrier scattering determines the operation and the performance of many semiconductor based devices like transistors, solar cells, or lasers [1–8]. At high carrier concentrations, e.g., effects like kinetic hole burning, carrier capture, and carrier relaxation govern the operation of semiconductor lasers [9–14]. Therefore, a detailed knowledge of scattering processes is of great interest for the optimization of many semiconductor devices. Ultrafast spectroscopy is a viable tool to gain insights into those scattering mechanisms. In the past, especially two methods were used to investigate scattering events between charge carriers and excitons experimentally. Those are optical pump-optical probe spectroscopy, in particular four-wave-mixing spectroscopy (FWM), and time-resolved photoluminescence (TRPL) spectroscopy [15–23]. In FWM experiments the scattering of charge carriers or incoherent excitons with coherent exciton polarizations has been investigated [24]. Here, scattering leads to a dephasing of the optically induced polarization. Accordingly, the dephasing time of a $1s$ exciton polarization is analyzed in the presence of an electron-hole plasma or incoherent excitons that can be injected by an additional prepulse [16,17,24]. Since the dephasing time is inversely connected to the homogeneous linewidth, the homogeneous line broadening of an excitonic transition also gives access to electron-exciton scattering. This is exploited in TRPL and optical transmission experiments by analyzing the linewidth of excitonic transitions [17,19,21,25–28]. Again, additional excitation pulses can be used to create the desired environment [17,19]. Unfortunately, by analyzing transition linewidths and/or dephasing times, the insights are limited to the influence of scattering events on discrete quantum states. A discrete state of, e.g., an exciton can already be destroyed by elastic scattering processes in which the exciton remains bound and only observes a change of momentum. However,

a destructive inelastic scattering process in which the exciton overcomes the attractive Coulomb interaction and breaks into an unbound electron-hole pair has the same effect as elastic scattering in these FWM or TRPL experiments [29]. Therefore, it is hard to distinguish between elastic and inelastic scattering processes with those methods. Consequently, little is known experimentally about destructive inelastic scattering, its efficiency, especially in comparison to elastic scattering processes, and how electron-exciton scattering affects the decay of exciton populations [30].

Another spectroscopic technique to study many-particle interactions is optical pump-terahertz probe spectroscopy. Since its pioneering works in the 1980s and early 90s [31–35], optical pump-terahertz probe spectroscopy has proven to be a powerful method for investigating intraband charge carrier interactions in semiconductors and their quasiparticles such as excitons [36–39]. Here, we use optical pump-terahertz probe spectroscopy to study the lifetime as well as the intraexcitonic linewidth of an incoherent exciton population under the impact of a hot electron-hole plasma. Therefore, a second optical pulse injects additional carriers which interact with an incoherent population of excitons that arose from a previous optical pulse. Probing the intraexcitonic $1s - 2p$ transition and analyzing its density-dependent decay and its linewidth after the arrival of the second optical pulse provides insights into the destructive inelastic as well as the total scattering rate. This enables the experimental differentiation between elastic and inelastic scattering processes.

II. EXPERIMENTAL DETAILS

The sample investigated is a piece of nominally undoped n -type germanium (Ge) with a thickness of $L = 500 \mu\text{m}$ and a room temperature resistivity larger than $30 \Omega \text{ cm}$. The sample is held at 10 K in a continuous flow liquid-He cryostat.

The experimental setup is schematically shown in Fig. 1(c). The experiment is performed with a 1 kHz titanium-sapphire-based regenerative amplifier system which provides 35 fs

^{*}markus.stein@physik.uni-marburg.de

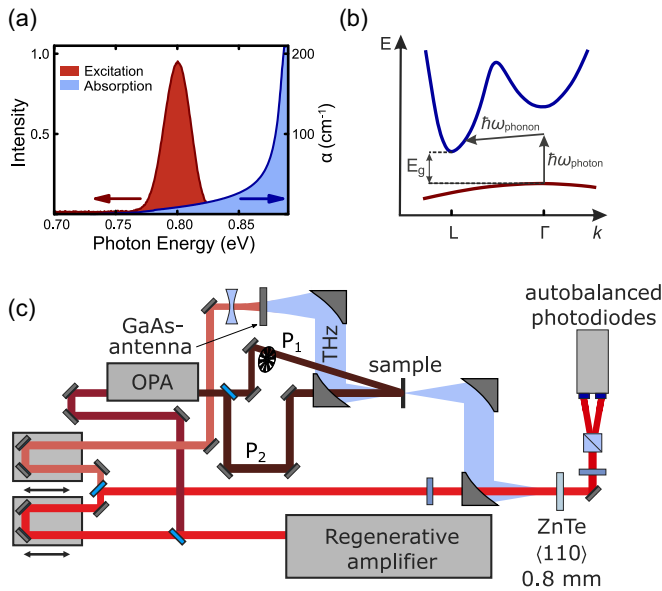


FIG. 1. (a) The linear absorption of the sample (blue) is plotted together with the spectrum of the optical excitation pulse (red). (b) Schematic of the excitation process and the indirect band structure of Ge. (c) A schematic of the experimental optical pump-THz probe setup. The THz section is purged with dry nitrogen gas to avoid THz absorption by water vapor.

pulses spectrally centered around 800 nm. This pulse train is split into three parts. One part of the pulse excites a LT-grown large aperture GaAs antenna. The antenna emits ~ 1 ps long terahertz (THz) pulses, which probe the sample's intraexcitonic $1s - 2p$ transition and, hence, indicate the presence of an incoherent exciton population. The second part of the pulse is used as a gate pulse to record the THz pulse via electro optical sampling in an $800 \mu\text{m}$ thick (110) cut ZnTe crystal [40,41]. A pair of autobalanced photodiodes is used to detect the THz field-induced changes of the gate pulse polarization which enables the sampling of the THz waveform. To get rid of water vapor absorption we purge the THz part of our setup with nitrogen gas. The photon energy of the third part of the pulse is converted in an optical parametric amplifier (OPA) to 0.795 eV (1560 nm) with a full width at half maximum (FWHM) of 31 meV and a pulse duration of roughly 60 fs. Thereafter, the pulse is split into two by a beam splitter. One part (P_1) is mechanically chopped and excites the Ge crystal under an angle of $\sim 20^\circ$. Since we optically excite the sample energetically below its direct band gap, the absorption coefficient is low with 7.5 cm^{-1} , which ensures a homogeneous excitation profile in propagation direction. This first pulse P_1 generates an electron-hole plasma, which after 6.7 ns has converted nearly completely into an incoherent population of excitons as previous experiments have shown [42]. With a time delay of 6.7 ns relative to the first optical pulse, the second pulse P_2 provides an additional excitation of the sample [see Fig. 1(c)]. This second beam again generates an electron-hole plasma that interacts with the incoherent population of excitons. In our experiment we can, hence, directly probe how the incoherent exciton population decays via scattering with free carriers. Furthermore, we can monitor

the linewidth of the intraexcitonic transition and follow the subsequent reformation of incoherent excitons.

Our setup allows us to detect THz pulses with a bandwidth ranging from 1–12 meV. A time window of 16.5 ps is measured with the THz pulse centered in the middle of this window. Afterwards, a Hanning window function is applied to the measured waveforms before Fourier transformation into the frequency domain. This yields the frequency domain fields of the reference pulse $E(\omega)$ and the pump-induced change $\Delta E(\omega)$ of the first excitation pulse. The absorption $\alpha(\omega)$ as well as the change of the real part of the dielectric function $\Delta\epsilon_1(\omega)$ are given by [43]

$$\alpha(\omega) = 2\Delta\sigma_1(\omega) = \frac{2}{L} \text{Re} \left(\frac{\Delta E(\omega)}{E(\omega) + \Delta E(\omega)} \right), \quad (1)$$

$$\Delta\epsilon_1(\omega) = \frac{2c_0\sqrt{\epsilon_r}}{\omega L} \text{Im} \left(\frac{\Delta E(\omega)}{E(\omega) + \Delta E(\omega)} \right), \quad (2)$$

where c_0 is the speed of light in vacuum and ϵ_r is the dielectric constant of the material.

In order to determine the specified photon densities, the knife-edge method has been used to measure the width of both the optical and the THz pulse. Under the assumption of perfect spatial overlap, it is determined which portion of the lateral 3 mm large optical pulse lies within the FWHM of the 1 mm large THz pulse. Together with the power of the optical pulse, which has been determined by a thermal power meter, the photon density per pulse ρ is calculated for the FWHM of the THz pulse. Using the spectrum of the optical pulse $I_0(\omega)$ and the measured linear absorption of the sample $\alpha(\omega)$, the absorption for each frequency is weighted with the respective intensity of the spectrum to obtain the average absorption of the optical pulse A_{avg} :

$$A_{\text{avg}} = \frac{\sum_{\omega} (I_0(\omega) - I_0(\omega) \cdot e^{-\alpha(\omega)L})}{\sum_{\omega} I_0(\omega)} = 0.293. \quad (3)$$

Together with the photon density ρ , the sample thickness L , and the reflectance R , the charge carrier density n can be calculated:

$$n = \frac{(\rho - \rho R) \cdot A_{\text{avg}}}{L}. \quad (4)$$

Here, a value of 0.36 is used for the reflectance of Ge.

III. RESULTS

To study the inelastic scattering process of an unbound electron-hole plasma with an incoherent exciton population, we analyze the response of the probing THz pulse shortly before and after the second optical pulse injects an electron-hole plasma. As the injected charge carriers collide with the existing exciton population different scattering mechanisms are possible [29,30,44,45]. An elastic scattering process may change the momentum and the kinetic energy of the exciton but will not destroy the Coulomb bound electron-hole pair [29,44]. Since the probing THz pulse detects intraexcitonic transitions from excitons of all center-of-mass momentums, such elastic scattering processes will hardly change the oscillator strength of the intraexcitonic transition.

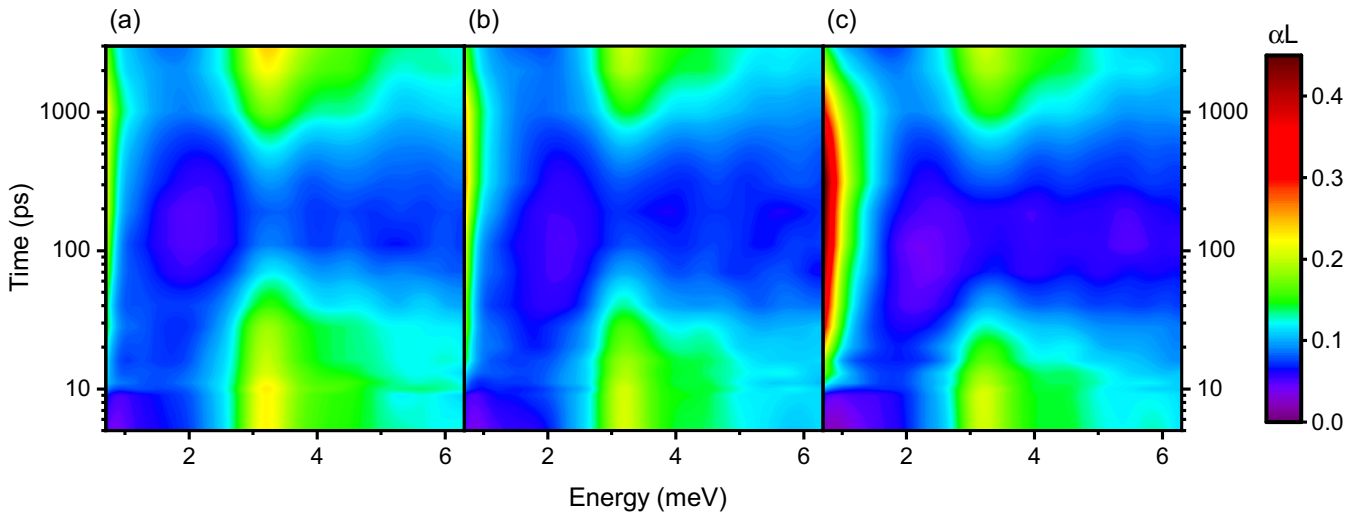


FIG. 2. Contour plots of the THz absorption for a constant photon density of the first excitation pulse P_1 of 9.8×10^{13} photons/cm² and photon densities of (a) 2.9×10^{13} photons/cm², (b) 5.9×10^{13} photons/cm², and (c) 1.0×10^{14} photons/cm² for the second optical pulse P_2 . The second pulse is delayed by 6.7 ns with respect to the first optical pulse. A time delay of zero between the second optical pulse and the THz pulse is set to 10 ps on the time axis to allow for a logarithmic representation. Before the second optical pulse excites the sample, all graphs show a pronounced intraexcitonic resonance at 3.2 meV. With the excitation from the second optical pulse at 10 ps, the amplitude of the resonance decreases on a time scale of tens of picoseconds, while simultaneously the absorption increases at low energies. This process occurs more rapidly with increasing photon density of the second pulse. It takes a few hundred picoseconds for the intraexcitonic resonance to build up again and about 3 ns to reach a similar level as before the excitation of the second pulse.

However, elastic scattering processes increase the linewidth of the transition. In contrast, destructive inelastic scattering processes overcome the Coulomb interaction and the exciton breaks into a free electron-hole pair [29]. As the plasma response of an unbound electron-hole pair differs significantly from intraexcitonic transitions, we are able to clearly identify the inelastic scattering by means of THz probe spectroscopy.

Figure 2 shows contour plots of the THz absorption for a photon density of 9.8×10^{13} photons/cm² from the first pulse and three different photon densities from the second pulse. The second optical pulse is delayed by 6.7 ns with respect to the first pulse and its arrival, i.e., a zero time delay between the second optical pulse and the THz probe pulse, is set to 10 ps on the time axis. Before the second pulse arrives an almost pure $1s$ exciton population has been built as the absorption peak at ~ 3.2 meV indicates. The second pulse then injects the electron-hole plasma at 10 ps. However, signatures of the intraexcitonic transitions remain and decay—depending on the photon density of the second pulse—on a time scale of tens to hundreds of picoseconds. Once intraexcitonic signatures decay, the plasma response increases as a rising absorption below 1.5 meV reveals. Here, the transition of the $1s$ exciton population into a free electron-hole plasma due to inelastic scattering is caught in the act. For lower photon densities of the second pulse, a small fraction of excitons survives as their signatures are still visible at hundreds of picoseconds [see Fig. 2(a)]. In contrast, higher photon densities lead to a complete decay of the exciton population. Several hundred picoseconds after the second pulse arrives, the electron-hole plasma is cooled down and the reformation of an exciton population starts. After 3 ns, an almost pure exciton population is restored.

A. Inelastic scattering rates

To obtain decay times of the exciton population different approaches are possible. One could analyze the plasma response after the second optical pulse excites the sample. When the exciton population decays into free electron-hole pairs via inelastic scattering, the plasma response increases. A readout of the transients of the absorption at a certain energy below the intraexcitonic resonance is well suited to monitor this increase of the plasma response. However, the plasma response depends on the effective mass of the charge carriers as well as on scattering events. Both are not necessarily constant in this dynamic environment. Therefore, we use another approach as the analysis of the plasma response might be biased.

The approach chosen here is to directly monitor the absorption of the intraexcitonic transitions. When excitons are destroyed by inelastic scattering, they no longer contribute to the intraexcitonic absorption. Hence, the intraexcitonic absorption strength decays. To account for imaginable shifts and broadening effects of intraexcitonic transitions, we integrate the absorption from 2.0 meV to 6.0 meV. In Fig. 3(a), we show the integrated intraexcitonic absorption, i.e., the intraexcitonic oscillator strength, for different time delays for a photon density of 9.8×10^{13} photons/cm² of the first pulse and four different densities of the second pulse (vertical offsets are added for clarity). When the second pulse arrives at 10 ps, a clear decay of the intraexcitonic oscillator strength is observed within the first 100 ps. This decay is based on the destruction of the exciton population by inelastic scattering with the electron-hole plasma that is created at 10 ps. By fitting simple biexponential functions we yield the decay times (τ_1) of the exciton population as well as its reformation times (τ_2). In Fig. 3(c), the decay times τ_1 (black data points) are shown for two different photon densities of the first optical pulse.

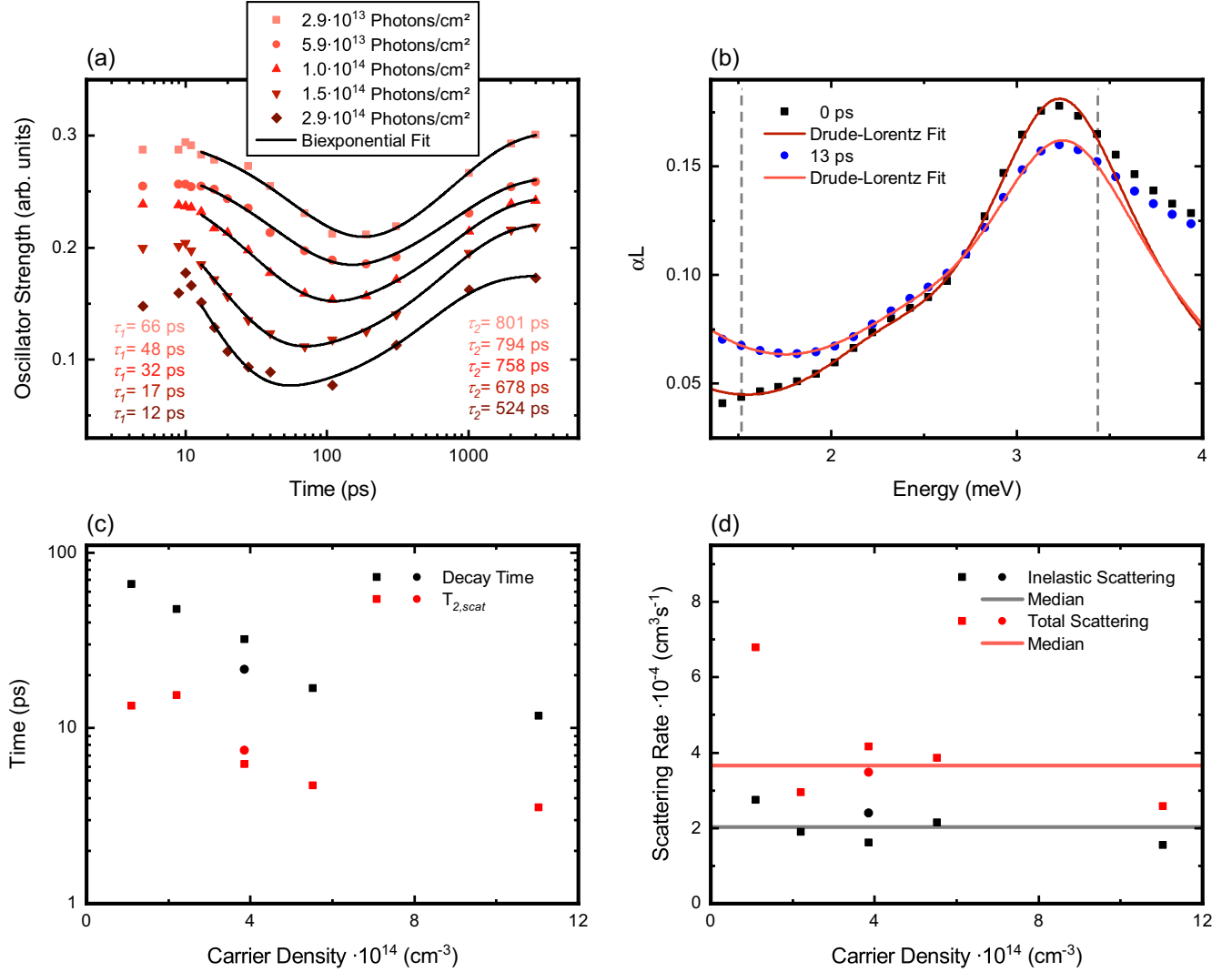


FIG. 3. (a) Intraexcitonic oscillator strength for a photon density of 9.8×10^{13} photons/cm² from the first optical pulse and five different densities of the second pulse. For the sake of clarity, the data points have been provided with an offset. A biexponential fit (black) yields the decay as well as the reformation times. (b) Fit of a Drude-Lorentz model to the intraexcitonic $1s - 2p$ transition 10 ps before and 3 ps after the second optical pulse injects an electron-hole plasma. The borders of the fit are marked by vertical gray dashed lines. (c) Decay times τ_1 (black data points) from the biexponential fit are plotted together with the additional dephasing due to electron-exciton scattering $T_{2,scat}$ (red data points), which is calculated via Eq. (7), for photon densities of 9.8×10^{13} photons/cm² (squares) and 2.8×10^{14} photons/cm² (circles) of the first excitation pulse. (d) The corresponding inelastic and total scattering rates together with the respective median of the data.

The decay times τ_1 are connected with the inelastic scattering rate γ_{in} via $\gamma_{in} = \frac{2}{\tau_1 \cdot n}$, where n is the electron density that is injected into the conduction band by the second optical pulse [24]. Doing so, we yield a median scattering rate of 2.0×10^{-4} cm³ s⁻¹ as shown in Fig. 3(d). This scattering rate is roughly an order of magnitude lower than those observed in Ref. [24] for electron-exciton scattering in bulk gallium arsenide (GaAs). As already stated, Ref. [24] measures the sum of elastic and inelastic scattering, i.e., the total scattering rate. The decay of the intraexcitonic transition investigated here, on the other hand, is only sensitive to inelastic scattering.

B. Linewidth of the intraexcitonic transition

Similar to TRPL or optical transmission experiments [17,19,25,26,28], we can investigate the linewidth of the

intraexcitonic transition before and after the second optical pulse generates an electron-hole plasma. Here, we use a phenomenological Drude-Lorentz model for a quantitative analysis of the measured spectra [46]. This approach describes the pump-induced changes of the frequency-dependent dielectric function $\Delta\epsilon(\omega) = \Delta\epsilon_1 + i\Delta\sigma_1/(\epsilon_0\omega)$ by means of two components

$$\Delta\epsilon(\omega) = \frac{n_x e^2}{L\epsilon_0\mu} \left(\frac{f_{1s-2p,\parallel}}{\frac{E_{res,\parallel}^2}{\hbar^2} - \omega^2 - i\omega\Delta_{hom}} + \frac{f_{1s-2p,\perp}}{\frac{E_{res,\perp}^2}{\hbar^2} - \omega^2 - i\omega\Delta_{hom}} \right) - \frac{e^2}{L\epsilon_0\mu} \times \frac{n_{fc}}{\omega + i\omega\Gamma}. \quad (5)$$

The first two terms consist of two Lorentzian resonances to account for the two distinct intraexcitonic $1s - 2p$ transitions that are caused by the anisotropy of L -valley electrons in bulk Ge [42,47,48]. Since the oscillator strengths $f_{1s-2p,\parallel}$ and $f_{1s-2p,\perp}$ are not determined exactly, we are free to use just one reduced mass μ and one $1s$ exciton density n_x for both oscillators. Furthermore, we assume that both resonances at energies $E_{\text{res},\parallel}$ and $E_{\text{res},\perp}$ have the same homogeneous linewidth Δ_{hom} . The last term represents the Drude response of the free electron-hole plasma. Here, we use just one total free carrier density n_{fc} and assume that we only have one scattering rate Γ . Thus, the remaining fitting parameters are the resonance energies $E_{\text{res},\parallel}$ and $E_{\text{res},\perp}$, the homogeneous linewidth Δ_{hom} , the carrier scattering rate Γ , and the exciton and free carrier densities n_x and n_{fc} . Additional constants in all terms are the electron charge e and the vacuum permeability ϵ_0 .

By fitting $2\epsilon_0\omega \cdot \text{Im}(\Delta\epsilon(\omega))$ to the experimentally determined absorption spectra as shown exemplarily for two time delays in Fig. 3(b), we receive the linewidth Δ_{hom} of the intraexcitonic $1s - 2p$ transition. Since the dephasing time T_2 is connected to the homogeneous linewidth Δ_{hom} via $T_2 = \frac{2}{\Delta_{\text{hom}}}$, the homogeneous line broadening of an intraexcitonic transition gives access to the dephasing due to electron-exciton scattering. Here, we determine the homogeneous linewidth 10 ps before and 3, 6, and 10 ps after the second optical pulse injects the electron-hole plasma. Then, to minimize the error, we average the linewidth for the three time delays (3, 6, and 10 ps) after the second optical excitation and calculate the dephasing time. The determined dephasing time T_2 is then composed of the natural dephasing time of the transition $T_{2,\text{nat}}$, which we obtain from the measurement 10 ps before the second pulse arrives, and the additional dephasing due to electron-exciton scattering $T_{2,\text{scat}}$ via [24]:

$$\frac{1}{T_2} = \frac{1}{T_{2,\text{nat}}} + \frac{1}{T_{2,\text{scat}}}. \quad (6)$$

Converting to $T_{2,\text{scat}}$ results in

$$T_{2,\text{scat}} = \frac{T_2 \cdot T_{2,\text{nat}}}{T_{2,\text{nat}} - T_2}. \quad (7)$$

The dephasing time due to additional scattering $T_{2,\text{scat}}$ is plotted in Fig. 3(c) (red data points) against the carrier density. However, the $1s - 2p$ transition consists of two excited states, namely the $1s$ and the $2p$ state, the lifetimes of which are shortened by the additional electron-exciton scattering. Accordingly, $T_{2,\text{scat}}$ consists of the additional dephasing of the $1s$ states ($T_{2,\text{scat},1s}$) as well as the $2p$ states ($T_{2,\text{scat},2p}$) [49]:

$$\frac{1}{T_{2,\text{scat}}} = \frac{1}{T_{2,\text{scat},1s}} + \frac{1}{T_{2,\text{scat},2p}}. \quad (8)$$

Since we only have access to the linewidth of the superposition of both states with THz spectroscopy, we have to make an assumption at this point. Assuming that both states are equally influenced by scattering we get:

$$T_{2,\text{scat},1s} = 2T_{2,\text{scat}}. \quad (9)$$

Herewith we are able to calculate the total scattering rate of the $1s$ exciton state γ_{tot} via:

$$\gamma_{\text{tot}} = \frac{2}{T_{2,\text{scat},1s} \cdot n} = \frac{1}{T_{2,\text{scat}} \cdot n}. \quad (10)$$

By using the median we receive a total electron-exciton scattering rate of $3.7 \times 10^{-4} \text{ cm}^3 \text{ s}^{-1}$ as shown in Fig. 3(d). This is roughly a factor of 4 smaller than the electron-exciton scattering rate as determined in Ref. [24] for GaAs. However, in Ref. [24] the scattering rate of optically excited excitonic polarizations with a center-of-mass momentum close to $\vec{K} = 0$ is determined, while we determine the scattering rate of an incoherent exciton population with different center-of-mass momentums. In contrast to Schultheis *et al.* [24], the scattering rate of large-momentum excitons is determined in Ref. [23]. With $9.5 \times 10^{-5} \text{ cm}^3 \text{ s}^{-1}$ the scattering rate from Ref. [23] is approximately a factor of 4 smaller than the scattering rate determined by us and a factor of 17 smaller than the scattering rate determined by Schultheis *et al.* They attribute their much lower scattering rate in comparison to Schultheis *et al.* to drastically reduced scattering of large-momentum excitons with free carriers [23]. Since our unique optical pump-terahertz probe method takes into account excitons of all center-of-mass momentums, it is very reasonable that the scattering rate determined by us lies just between the two values of Ref. [23] and Ref. [24].

The total scattering rate is composed of elastic and inelastic scattering. Since we are able to determine the inelastic scattering rate by the decay of the exciton population, we now have access to the elastic scattering rate as well. The elastic scattering rate is equivalent to the difference between the total and the inelastic scattering rate. This gives us an elastic scattering rate of $1.7 \times 10^{-4} \text{ cm}^3 \text{ s}^{-1}$. Thus, for the excitation conditions used here with an excess energy of the electron-hole plasma of $\sim 50 \text{ meV}$, the elastic scattering rate is comparable to the inelastic scattering rate of $2.0 \times 10^{-4} \text{ cm}^3 \text{ s}^{-1}$.

C. Exciton reformation

After the exciton population has been destroyed by inelastic scattering, the reformation process begins. However, in contrast to the observations for a single excitation pulse that are described in Ref. [42], the exciton formation process is not delayed but starts instantaneously after the exciton population is destroyed. Thus, the scattering and the reformation processes can be described by a simple biexponential fit as shown in Fig. 3(a). For a single excitation pulse, the hot electron-hole plasma has to cool down first via phonons before excitons can form. However, when a second pulse generates a hot electron-hole plasma in the presence of an incoherent exciton population, the plasma can efficiently cool down via inelastic electron-exciton scattering. As a result, a cold electron-hole plasma is present after the scattering, so that the exciton formation can start immediately. In agreement with the findings from Ref. [42], the excitation with a second optical pulse confirms that the exciton formation is faster at higher charge carrier densities. In Fig. 3(a) the reformation time τ_2 decreases continuously from 801 ps for the lowest photon density of the second pulse of $2.9 \times 10^{13} \text{ photons/cm}^2$ to 524 ps for the highest photon density of $2.9 \times 10^{14} \text{ photons/cm}^2$. The

photon densities correspond to charge carrier densities of $1.1 \times 10^{14} \text{ cm}^{-3}$ and $1.1 \times 10^{15} \text{ cm}^{-3}$, respectively, which are at least one order of magnitude below the Mott transition in Ge [50]. A comparison with the formation times from Ref. [42] shows that at the same charge carrier densities the observed exciton formation is much faster here. This may indicate that even though the initial exciton population is destroyed by inelastic scattering, the reformation process of excitons finds much more favorable conditions than the exciton formation out of an optically excited electron-hole plasma.

IV. CONCLUSION

In conclusion, we present a unique method to experimentally get access to both destructive inelastic and elastic electron-exciton scattering via optical pump-terahertz probe spectroscopy. We monitor the decay of the intraexcitonic

transitions of an incoherent exciton population by scattering with an electron-hole plasma which is generated by a second optical pulse in bulk Ge. By analyzing the decay times, we find an inelastic scattering rate of $2.0 \times 10^{-4} \text{ cm}^3 \text{ s}^{-1}$. An analysis of the linewidth broadening of the intraexcitonic $1s - 2p$ transition due to the arrival of the second optical pulse yields a total scattering rate of $3.7 \times 10^{-4} \text{ cm}^3 \text{ s}^{-1}$. The difference between total and inelastic scattering rate results in the elastic scattering rate, which is $1.7 \times 10^{-4} \text{ cm}^3 \text{ s}^{-1}$ accordingly. The following reformation of the exciton population is accelerated for higher charge carrier densities.

ACKNOWLEDGMENT

Financial support from the Deutsche Forschungsgemeinschaft via the Collaborative Research Center SFB 1083 is gratefully acknowledged.

-
- [1] V. Gantmakher and Y. Levinson, *Carrier Scattering in Metals and Semiconductors*, Modern Problems in Condensed Matter Sciences (Elsevier Science, Amsterdam, 2012).
- [2] D. Derkacs, S. H. Lim, P. Matheu, W. Mar, and E. T. Yu, *Appl. Phys. Lett.* **89**, 093103 (2006).
- [3] J. Xiang, W. Lu, Y. Hu, Y. Wu, H. Yan, and C. M. Lieber, *Nature (London)* **441**, 489 (2006).
- [4] K. Natori, *J. Appl. Phys.* **76**, 4879 (1994).
- [5] S. Takagi, J. L. Hoyt, J. J. Welsler, and J. F. Gibbons, *J. Appl. Phys.* **80**, 1567 (1996).
- [6] R. Köhler, A. Tredicucci, F. Beltram, H. E. Beere, E. H. Linfield, A. G. Davies, D. A. Ritchie, R. C. Iotti, and F. Rossi, *Nature (London)* **417**, 156 (2002).
- [7] P. Palestri, D. Esseni, S. Eminent, C. Fiegna, E. Sangiorgi, and L. Selmi, *IEEE Trans. Electron Devices* **52**, 2727 (2005).
- [8] D. Hofstetter, M. Beck, T. Aellen, and J. Faist, *Appl. Phys. Lett.* **78**, 396 (2001).
- [9] R. Binder, D. Scott, A. E. Paul, M. Lindberg, K. Henneberger, and S. W. Koch, *Phys. Rev. B* **45**, 1107 (1992).
- [10] T. R. Nielsen, P. Gartner, and F. Jahnke, *Phys. Rev. B* **69**, 235314 (2004).
- [11] W. Chow, A. Girndt, and S. Koch, *Opt. Express* **2**, 119 (1998).
- [12] M. Hilpert, H. Klann, M. Hofmann, C. Ellmers, M. Oestreich, H. C. Schneider, F. Jahnke, S. W. Koch, W. W. Rühle, H. D. Wolf, D. Bernklau, and H. Riechert, *Appl. Phys. Lett.* **71**, 3761 (1997).
- [13] M. van der Poel, E. Gehrig, O. Hess, D. Birkedal, and J. M. Hvam, *IEEE J. Quantum Electron.* **41**, 1115 (2005).
- [14] G. Malpuech, A. Kavokin, A. Di Carlo, and J. J. Baumberg, *Phys. Rev. B* **65**, 153310 (2002).
- [15] J. Shah, *Ultrafast Spectroscopy of Semiconductors and Semiconductor Nanostructures*, Springer Series in Solid-State Sciences (Springer, Berlin, Heidelberg, 2013).
- [16] A. Honold, L. Schultheis, J. Kuhl, and C. W. Tu, *Phys. Rev. B* **40**, 6442 (1989).
- [17] M. Koch, R. Hellmann, G. Bastian, J. Feldmann, E. O. Göbel, and P. Dawson, *Phys. Rev. B* **51**, 13887 (1995).
- [18] R. Hellmann, M. Koch, J. Feldmann, S. T. Cundiff, E. O. Göbel, D. R. Yakovlev, A. Waag, and G. Landwehr, *Phys. Rev. B* **48**, 2847 (1993).
- [19] A. Manassen, E. Cohen, A. Ron, E. Linder, and L. N. Pfeiffer, *Phys. Rev. B* **54**, 10609 (1996).
- [20] V. Capozzi, L. Pavesi, and J. L. Staehli, *Phys. Rev. B* **47**, 6340 (1993).
- [21] D. Huang, H. Y. Chu, Y. C. Chang, R. Houdré, and H. Morkoç, *Phys. Rev. B* **38**, 1246 (1988).
- [22] G. Göger, M. Betz, A. Leitenstorfer, M. Bichler, W. Wegscheider, and G. Abstreiter, *Phys. Rev. Lett.* **84**, 5812 (2000).
- [23] M. Betz, G. Göger, A. Leitenstorfer, M. Bichler, G. Abstreiter, and W. Wegscheider, *Phys. Rev. B* **65**, 085314 (2002).
- [24] L. Schultheis, J. Kuhl, A. Honold, and C. W. Tu, *Phys. Rev. Lett.* **57**, 1635 (1986).
- [25] R. C. C. Leite, J. Shah, and J. P. Gordon, *Phys. Rev. Lett.* **23**, 1332 (1969).
- [26] W. Liu, D. Jiang, K. Luo, Y. Zhang, and X. Yang, *Appl. Phys. Lett.* **67**, 679 (1995).
- [27] H. Wang, K. Ferrio, D. G. Steel, Y. Z. Hu, R. Binder, and S. W. Koch, *Phys. Rev. Lett.* **71**, 1261 (1993).
- [28] D. R. Wake, H. W. Yoon, J. P. Wolfe, and H. Morkoç, *Phys. Rev. B* **46**, 13452 (1992).
- [29] G. Ramon, A. Mann, and E. Cohen, *Phys. Rev. B* **67**, 045323 (2003).
- [30] S. Elkomoos and G. Munschy, *J. Phys. Chem. Solids* **40**, 431 (1979).
- [31] D. H. Auston, K. P. Cheung, J. A. Valdmanis, and D. A. Kleinman, *Phys. Rev. Lett.* **53**, 1555 (1984).
- [32] P. R. Smith, D. H. Auston, and M. C. Nuss, *IEEE J. Quantum Electron.* **24**, 255 (1988).
- [33] R. Sprik, I. N. Duling, C. Chi, and D. Grischkowsky, *Appl. Phys. Lett.* **51**, 548 (1987).
- [34] B. I. Greene, J. F. Federici, D. R. Dykaar, A. F. J. Levi, and L. Pfeiffer, *Opt. Lett.* **16**, 48 (1991).
- [35] R. Groeneveld and D. Grischkowsky, *JOSA B* **11**, 2502 (1994).
- [36] R. Huber, F. Tausler, A. Brodschelm, M. Bichler, G. Abstreiter, and A. Leitenstorfer, *Nature (London)* **414**, 286 (2001).
- [37] R. A. Kaindl, M. A. Carnahan, D. Hägele, R. Löwenich, and D. S. Chemla, *Nature (London)* **423**, 734 (2003).
- [38] T. Suzuki and R. Shimano, *Phys. Rev. Lett.* **103**, 057401 (2009).

- [39] M. Stein, C. Lammers, P.-H. Richter, C. Fuchs, W. Stolz, M. Koch, O. Vänskä, M. J. Weseloh, M. Kira, and S. W. Koch, *Phys. Rev. B* **97**, 125306 (2018).
- [40] Q. Wu and X. Zhang, *Appl. Phys. Lett.* **67**, 3523 (1995).
- [41] A. Nahata, A. S. Weling, and T. F. Heinz, *Appl. Phys. Lett.* **69**, 2321 (1996).
- [42] M. Stein, C. Lammers, P. Springer, P.-H. Richter, S. W. Koch, M. Koch, and M. Kira, *Phys. Rev. B* **95**, 155207 (2017).
- [43] R. Ulbricht, E. Hendry, J. Shan, T. F. Heinz, and M. Bonn, *Rev. Mod. Phys.* **83**, 543 (2011).
- [44] S. Elkomoss and G. Munschy, *J. Phys. Chem. Solids* **38**, 557 (1977).
- [45] Y. Feng and H. N. Spector, *Superlattices Microstruct.* **3**, 459 (1987).
- [46] P. Steinleitner, P. Merkl, P. Nagler, J. Mornhinweg, C. Schüller, T. Korn, A. Chernikov, and R. Huber, *Nano Lett.* **17**, 1455 (2017).
- [47] P. Springer, S. W. Koch, and M. Kira, *J. Opt. Soc. Am. B* **33**, C30 (2016).
- [48] M. Stein, C. Lammers, J. T. Steiner, P.-H. Richter, S. W. Koch, M. Koch, and M. Kira, *J. Phys. B: At., Mol. Opt. Phys.* **51**, 154001 (2018).
- [49] D. Andrews and A. Demidov, *An Introduction to Laser Spectroscopy: Second Edition* (Springer US, New York, 2012).
- [50] F. Sekiguchi and R. Shimano, *Phys. Rev. B* **91**, 155202 (2015).